Journal of Electronic Materials (2021) 50:4599–4605
https://doi.org/10.1007/s11664-021-09001-8

ORIGINAL RESEARCH ARTICLE

An Experimental Study of the Dynamic Resistance in Surface Leakage Limited nBn Structures Based on HgCdTe Grown by Molecular Beam Epitaxy

A. V. Voitsekhovskii[1] · S. N. Nesmelov[1] · S. M. Dzyadukh[1] · S. A. Dvoretsky[1,2] · N. N. Mikhailov[2] · G. Y. Sidorov[2] · M. V. Yakushev[2]

Received: 27 June 2020 / Accepted: 7 May 2021 / Published online: 25 May 2021

Abstract
Mid-wave infrared nBn structures based on HgCdTe grown by molecular beam epitaxy on GaAs (013) substrates were fabricated. The composition in the absorbing layer was 0.29, and in the barrier layer it was 0.67. It was shown that the dark currents of the created nBn structures are limited by the surface leakage component. To study the bulk component of the dark current, it was proposed to use the admittance measurements of test metal-insulator-semiconductor (MIS) devices based on fabricated nBn structures in the case of the formation of a backward contact to the absorbing layer. It was established that surface leakage does not affect the dynamic resistance of the MIS device barrier. The dependence of the dynamic resistance of the barrier layer (R_b) of the MIS device in the accumulation mode on the area of the front electrode (A), voltage, and temperature was determined. It was shown that, with the exclusion of surface leakage, the values of the R_bA product in a temperature range of 230–300 K at forward biases are determined by the diffusion current of holes from the contact layer, and at reverse biases, by the diffusion current from the absorbing layer. It was found that at temperatures of 210–300 K, R_bA values exceeding the values of this parameter determined according to the empirical model Rule 07 were realized in the fabricated structures.

Keywords HgCdTe · molecular beam epitaxy · MWIR · unipolar barrier detectors · nBn structure · MIS device · dark current

Introduction

Mercury cadmium telluride is one of the most promising materials for creating third-generation infrared detectors.[1–3] The use of unipolar barrier structures for detection (for example, in the nBn configuration[4]) makes it possible to increase the operating temperature of photosensitive devices due to the suppression of some components of the dark current (Shockley–Read generation current and surface leakage current). The greatest successes have been achieved so far with the creation of III-V-based barrier detectors,[5–8] which is associated with the possibility of eliminating the barrier for minority charge carriers (photocarriers) while suppressing the current of the majority charge carriers. It has been theoretically shown that the creation of HgCdTe-based nBn detectors provides significant technological advantages[9–12] compared to traditional photodiodes, but there are still few attempts to implement such structures based on HgCdTe grown by molecular beam epitaxy (MBE).[13–15] The characteristics of the first MBE HgCdTe detectors for the spectral range 3–5 μm (mid-wave infrared [MWIR]) had large dark currents.[13,15] Somewhat great successes were achieved with the creation of barrier detectors based on HgCdTe grown by the metalorganic chemical vapor deposition (MOCVD) method.[16] Recently, MWIR nBn structures were fabricated based on HgCdTe MBE with diffusion-limited dark current in a temperature range of 180–300 K[17,18] and turn-on voltage of about −1 V.

The practical implementation of effective barrier detectors based on various material systems requires the

✉ S. N. Nesmelov
nesm69@mail.ru

[1] National Research Tomsk State University, 36 Lenina Ave., Tomsk, Russia 634050

[2] Rzhanov Institute of Semiconductor Physics SB RAS, 13 Lavrentiev Ave., Novosibirsk, Russia 630090

development of technologies for creating multilayer epitaxial systems, as well as the development of methods for the electrical characterization of such systems. In this case, one of the most important characteristics of unipolar barrier structures, including those with nBn design, is the dark current, which can be determined by the bulk component, the nature of which is different when using different materials, or the surface leakage component. Zero-bias dynamic resistance-area product values are closely related to dark current mechanisms and determine the noise properties of infrared detectors. This parameter is widely used to assess the quality of unipolar barrier detectors.[19,20]

Currently, studies of the mechanisms of dark current in nBn detectors based on materials III–V are being intensively carried out,[21–24] and new experimental methods are being developed for studying processes in multilayer unipolar systems.[25–28] An important task is the separation of the bulk and surface components of the dark current flowing through the nBn detector under various conditions. To solve this problem, measurements of the dependence of current density[13,17,23] or dynamic resistance[29,30] are usually used for nBn structures with different perimeter to area ratios (*P*/*A*). These methods are very laborious and do not provide high accuracy when one of the components of the dark current dominates. The analytical approach to isolating the contribution of surface leakage current from bulk dark current by simulating the current–voltage characteristic of InAs/GaSb superlattice detectors is known.[31] It seems to us that new possibilities for the separation of dark current components are provided by measurements of admittance, which were rarely used before in studies of the properties of nBn structures.[32–34] Recently, it was proposed to use metal–insulator–semiconductor (MIS) structures to study processes in unipolar barrier detectors.[35–37] An obvious application of MIS devices is the study of dopant concentration in the surface region of the adjacent semiconductor layer.[36] New possibilities are provided by the admittance measurements of MIS devices based on nBn structures during the formation of a backward contact to the absorbing layer (mesa configuration).[35,37] This is because the maximum width of the space charge region in MIS structures is much smaller than the distance from the edges of the frontal electrode to the sidewalls of the mesa structure. It can be assumed that measurements of the admittance of test MIS structures will allow us to study the dynamic resistance of the barrier layer in the nBn structure. In Ref. 37, preliminary studies of the admittance of MIS devices based on longwave infrared (LWIR) and MWIR nBn structures from MBE HgCdTe were carried out.

This work compares the results of studies of the dark current of MWIR nBn structures based on MBE HgCdTe and the admittance of test MIS structures made on the basis of such nBn structures.

Experimental Procedures

Heteroepitaxial HgCdTe films were grown by molecular beam epitaxy at the ISP SB RAS.[38] In the growth chamber for buffer layers on a preliminarily prepared atomically smooth and clean GaAs (013) substrate, ZnTe and CdTe buffer layers were sequentially grown using atomic flows of zinc (Zn) and cadmium (Cd) and fluxes of tellurium (Te_2). Buffer layers of ~ 50 nm were grown for ZnTe with the growth rate of 1.5 nm/s and ~ 5.0 μm for CdTe with the growth rate of 2 μm/h and growth temperature of the buffer layers was ~ 280°C. Further, in a separate growth chamber, solid solutions of mercury cadmium telluride were grown. HgCdTe growth was carried out from separate effusion sources of atomic fluxes of cadmium, mercury, and molecular flux of tellurium. The substrate temperature during the entire growth was constant ~ 180°C. The growth rate was determined from ellipsometric measurements at the initial stage of growth and was constant throughout the entire process at 1.49 μm per hour. The composition of the growing layer was changed by changing the cadmium flux using a mechanical shutter (opening/closing), both at the initial stage of growth (graded-gap layer) and during the growth of the barrier and contact layers. The thicknesses and compositions of the growing layers were monitored from in situ ellipsometric measurements. Then a graded-gap $Hg_{1-x}Cd_xTe$ layer with the thickness of about 1 μm was deposited on top of the CdTe layer. The working region of the nBn structure consisted of an absorbing layer, a barrier layer, and a contact layer. The composition in the absorbing layer with the thickness of about 2.5 μm was 0.29. The 120 nm thick wide-gap $Hg_{0.33}Cd_{0.67}Te$ layer was used as a barrier. The thickness of the $Hg_{0.67}Cd_{0.33}Te$ contact layer was about 140 nm. The concentration of indium donor impurity in all layers of the working region was 3.81×10^{15} cm^{-3}. Figure 1 shows the layout of the layers in the fabricated nBn structure. For the physical separation of various nBn structures, mesa structures were formed by etching the HgCdTe film in 0.5% solution of Br in HBr to an absorbing layer.

To passivate the sidewalls of the mesa structure, an Al_2O_3 dielectric film was deposited by plasma-enhanced atomic layer deposition.[39,40] A temperature of 120°C was chosen for applying the Al_2O_3 dielectric coating, since at this temperature mercury begins to evaporate from the surface of HgCdTe in vacuum, which violates the composition of the near-surface region. The temperature of 120°C is lower than the temperature of the trimethylaluminum (TMA) window (from 200°C to 300°C), but there is a lot of data about the possibility of growth of a stoichiometrically correct Al_2O_3

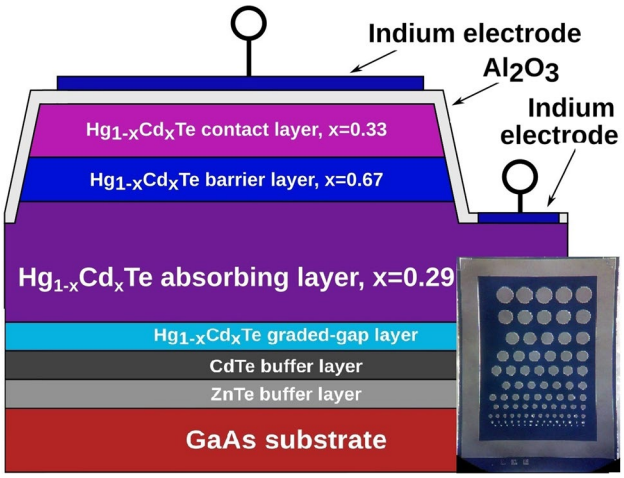

Fig. 1 Schematic representation of the test MIS device based on the nBn structure. In the inset is a photograph of the fabricated sample

film at a low temperature. Then, a local etching of the dielectric was carried out using a mixture of hydrofluoric acid and ammonium fluoride to create a contact frame that acts as a reverse contact.

For research, device structures of two types were created: nBn structures and MIS devices based on nBn structures. To form front contacts in nBn structures, an additional etching of the Al_2O_3 insulator was performed. During the fabrication of the MIS devices in the mesa configuration[35] no dielectric was etched, and the front contacts were deposited on top of the about 80 nm thick Al_2O_3 film. The front electrodes and the contact frame were created by applying indium using thermal spraying, and the temperature of the sample in this process did not exceed 100°C. Front electrodes had different diameters: from 20 μm to 500 μm (inset to Fig. 1). Most of the experimental results presented were obtained with the mesa diameter of the structure of 250 μm. The diameter of the front electrode was 230 μm for this structure.

Dark current and admittance measurements were performed on an automated setup based on the Agilent E4980A immittance meter, Lake Shore temperature controller, and Janis non-optical cryostat. The measurements were carried out in a temperature range from 10 K to 300 K. The error in measuring the dark current was about 1 nA. The admittance of MIS devices based on nBn structures was measured when the bias voltage changed from −5 V to 5 V in the frequency range from 500 Hz to 2 MHz.

Results and Discussion

Dark Current Study

Figure 2a shows the current–voltage (*I–V*) characteristics of the fabricated MWIR nBn structure based on the MBE HgCdTe measured at different temperatures. It can be seen from Fig. 2a that the *I–V*s are almost symmetric at forward and reverse biases. For the fabricated sample, a weak temperature dependence of the dark current is observed (similar to[13]). Figure 2b shows the dependence of the dark current density on the ratio of the mesa structure perimeter to its area (*P/A*) at a voltage of −2 V and temperature of 300 K. Fig. 2b shows that the dark current at reverse bias is limited by the surface leakage component.

The total current density through the nBn structure can be written as follows:

$$J = J_B + \frac{P}{A} J_S, \tag{1}$$

where J_B is the bulk current density proportional to the device area (in A/cm^2), J_S is the surface leakage current density per unit length of the perimeter (in A/cm). From the expression (1) it follows that the total current density linearly depends on the *P/A* ratio. From the slope of the linear approximation of the experimental points, the value of J_S

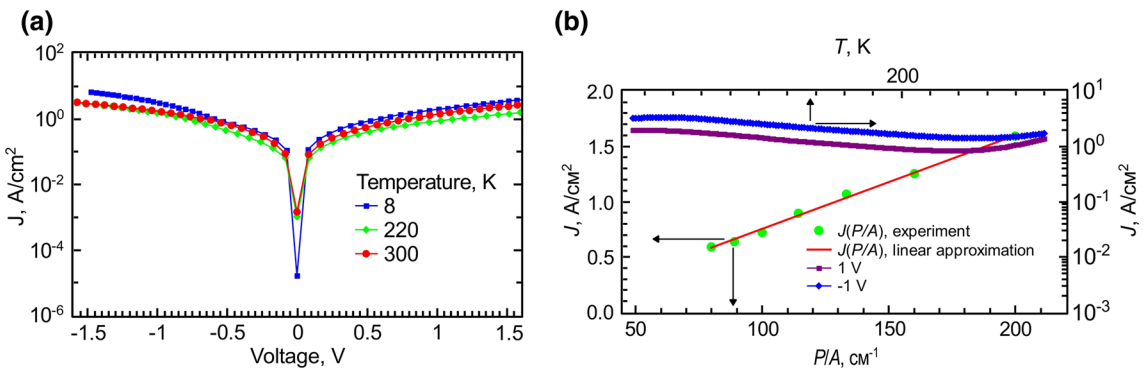

Fig. 2 (a) The *I–V* characteristics of the nBn structure at different temperatures and (b) the dependence of the dark current density on temperature and on the ratio of the structure mesa perimeter to area.

can be determined, and the value of J_B can be found from the intersection with the axis. The determined surface leakage current density (J_S) was 0.00848 A/cm. It is problematic to determine the bulk current density values from dark current measurements due to the dominance of the surface leakage component.

It can be noted that for MWIR nBn structures based on MBE HgCdTe with Al_2O_3 passivation with the composition in the barrier layer equal to 0.84, a diffusion-limited dark current was observed.[17,18] In this paper, we present experimental results for an nBn structure with the lower composition of 0.67 in the working layer. The role of surface leakage increases in such structures, but with a close composition in the barrier, the maximum values of the detectivity can be realized, which was previously shown theoretically.[41,42]

Admittance of the Test MIS Devices

In Fig. 3a, the symbols show the frequency dependence of the real and imaginary parts of the impedance of the MIS device based on the nBn structure, measured at a voltage of 2 V and temperature of 220 K. For admittance measurements, a parallel *R*-*C* equivalent circuit was used, which is easy to convert to a serial R_s–C_s circuit, which is used to determine the impedance. Parallel and serial equivalent circuits are shown in the inset to Fig. 3a. In Fig. 3b, the symbols show the experimental frequency dependence of the capacitance (C) and normalized conductance (G/ω, $G = 1/R$) of the MIS device, measured at a voltage of 2 V and temperature of 220 K.

To analyze processes in MIS devices based on nBn structures, the equivalent circuit method was used. The experimental frequency dependence of the admittance (or impedance) was compared with the theoretical dependence calculated using the equivalent circuit of the MIS device based on the nBn structure.

For calculating the frequency dependence of the impedance or admittance, the equivalent circuit of the MIS device was used, including the capacitance (C_d) and resistance (R_d) of the Al_2O_3 dielectric layer and the surface layer of the semiconductor, the capacitance (C_b) and resistance (R_b) of the barrier layer, and the series resistance of the absorbing layer (R_{bulk}). The resistance of the contact layer can be neglected due to its small values associated with the small thickness of this layer. The equivalent circuit shown in the inset to Fig. 3b is valid for the strong accumulation mode. In this case, the elements C_d and R_d characterize only the properties of the dielectric Al_2O_3 layer. In depletion and inversion modes, the capacitance C_d describes the series-connected capacitances of the dielectric and the surface layer of the semiconductor.[35]

In the calculations, the equivalent circuit of the MIS device in the accumulation mode, shown in the inset in Fig. 3b, was used. The calculation of the capacitance and resistance of the MIS device based on nBn structure with a serial equivalent circuit can be performed using the following expressions:

$$C_s = \left(\frac{\omega^2 C_d R_d^2}{1 + \omega^2 C_d^2 R_d^2} + \frac{\omega^2 C_b R_b^2}{1 + \omega^2 C_b^2 R_b^2} \right)^{-1}, \tag{2}$$

$$R_s = R_{bulk} + \frac{R_b}{1 + \omega^2 C_b^2 R_b^2} + \frac{R_d}{1 + \omega^2 C_d^2 R_d^2}, \tag{3}$$

where ω is the angular frequency of the test signal (ω=2πf, where f is the frequency in Hz).

The impedance of the MIS device can be written as follows:

$$Z(\omega) = \mathrm{Re}Z + j\mathrm{Im}Z = R_s - j\frac{1}{\omega C_s}, \tag{4}$$

A serial R_S–C_S chain can be converted to a parallel *R*–*C* chain using the following expressions:

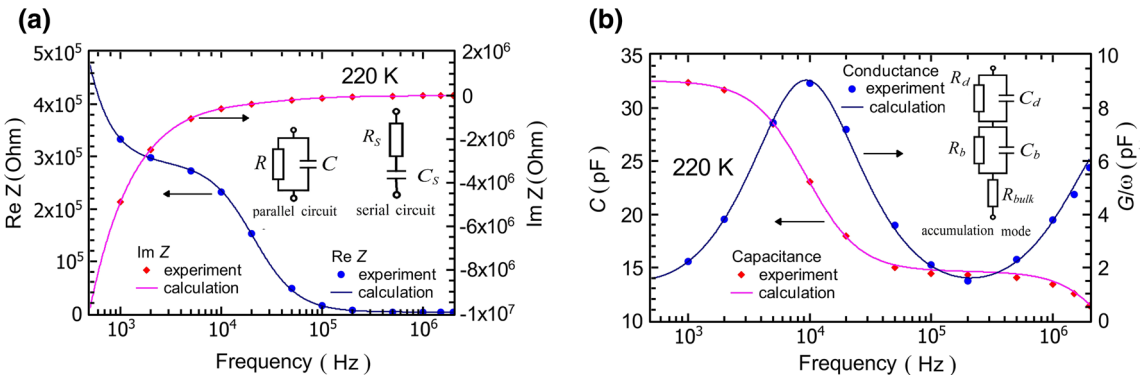

Fig. 3 (a) Experimental (symbols) and calculated (lines) frequency dependence of the real and imaginary parts of the impedance of the MIS device based on the nBn structure, and (b) experimental (symbols) and calculated (lines) dependence of the capacitance and normalized conductance of the nBn structure. The insets show parallel and serial equivalent circuits and the equivalent circuit of the MIS device in accumulation mode

$$C = \frac{C_s}{1+\omega^2 C_s^2 R_s^2}, \quad G = \frac{\omega^2 C_s^2 R_s}{1+\omega^2 C_s^2 R_s^2} \tag{5}$$

The Levenberg–Marquardt algorithm was used to determine the values of the elements of the equivalent circuit. The lines in Fig. 3a and b show the calculated dependence for the following values of the elements of the equivalent circuit: C_d = 32.63 pF, C_b = 26.79 pF, R_b = 285 kOhm, R_{bulk} = 2320 Ohm. Using the described methodology, it is possible to determine the values of the elements of the equivalent circuit under various conditions.

Figure 4 shows the dependence of the capacitances and resistance of the equivalent circuit on the area of the front electrode of the MIS device based on the nBn structure, determined at a temperature of 300 K and voltage of 2 V. It can be seen that the capacitances C_d and C_b are directly proportional to the area A. The resistance of the barrier layer R_b decreases with increasing area A, and the values of the series resistance of the absorbing layer do not depend on the area A, but are determined by the conductivity of the absorbing layer and the relative position of the front electrode and the contact frame, which acts as the backward electrode of the MIS device. The voltage dependence of the values of the equivalent circuit elements was determined and showed that most of the bias voltage drops on the dielectric layer. Therefore, the found resistance values are very close to zero-bias dynamic resistance of the nBn structures.

Thus, from the experimental frequency dependence of the impedance of the MIS device in the frequency range used, it is possible to accurately determine the value of the dynamic resistance of the barrier layer. It is essential that this resistance of the barrier layer depends only on the bulk component of the dark current, and surface leakage does not affect the admittance measurement results.

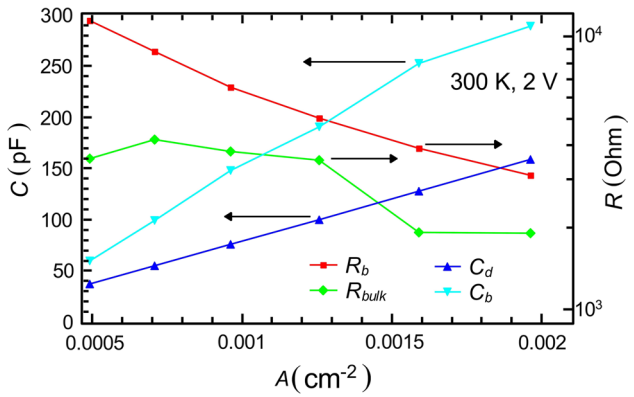

Fig. 4 Dependence of the values of the elements of the equivalent circuit on the area, determined at a temperature of 300 K and voltage of 2 V

The Investigation of the Dynamic Resistance of the Barrier Layer

Figure 5a shows the temperature dependence of the dynamic resistance of the barrier layer R_b determined at different bias voltages. It can be seen from the figure that for all biases, the resistance R_b increases significantly with cooling from 300 K to 220 K. With a decrease in the temperature from 220 K to 110 K, the resistance R_b increases slightly, but the dependence of this resistance on temperature becomes gentler. At lower temperatures, the dynamic resistance is practically independent of temperature. It should be noted that with large values of resistance, the accuracy of its determination decreases. Figure 5a also shows Arrhenius plots in the high temperature range at various voltages. The activation energy at forward biases is 0.331–0.334 eV, which is in good agreement with the band gap energy of the $Hg_{0.67}Cd_{0.33}Te$ contact layer (0.331 eV at 300 K). For reverse biases, the activation energy is 0.277–0.285 eV, which is close to the energy of the band gap of the absorbing layer (0.277 eV at 300 K). Thus, the resistance of the barrier layer at high temperatures

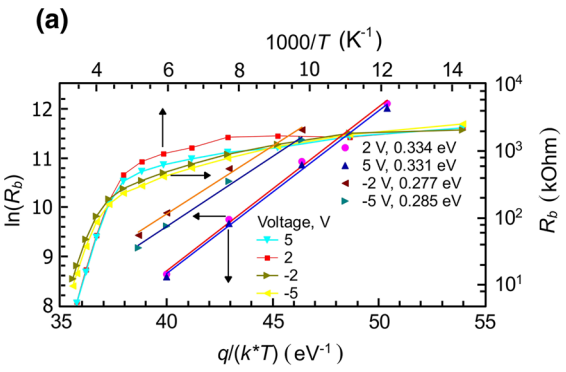

Fig. 5 (a) Temperature dependence of the barrier resistance and Arrhenius plots for various voltages and (b) temperature dependence of the product R_bA at reverse biases and calculation results according to the empirical model Rule 07. The inset shows the dependence of $1/(R_bA)$ value on the P/A ratio at a voltage of 2 V and temperature of 300 K

is determined by the diffusion of minority charge carriers (holes) from the absorbing layer at reverse biases, as well as the diffusion of holes from the contact layer at forward biases. It can be concluded that the barrier layer effectively prevents the flow of electrons at forward and reverse biases. It can be noted that according to the admittance measurements of MIS devices, the resistance R_b is limited by the bulk component of the current, and according to the current measurements, the dark current through the nBn structure is limited by surface leakage. Note that the radius of the mesa of the structure is 10 μm larger than the radius of the front electrode of the test MIS device. The maximum width of the space charge region, which is achieved in the strong inversion mode, is about 0.135 μm. Therefore, the electric field does not reach the sidewalls of the mesa structure. Because of this, surface leakage does not affect the measured impedance of the MIS device and the values of R_b are determined only by the bulk component of the dark current.

The inset in Fig. 5b shows the dependence of the value of R_bA, determined at a voltage of −2 V, on the ratio of the perimeter of the structure mesa to the area (P/A). The following expression can be written[30]:

$$\frac{1}{R_bA} = \frac{1}{(RA)_{bulk}} + \frac{1}{R_{surface}}\frac{P}{A}, \quad (6)$$

where $(RA)_{bulk}$ is the contribution of the bulk current component in Ohm × cm^2, $R_{surface}$ is the surface resistance in Ohm × cm. For the fabricated nBn structure at 300 K, the values of (RA) were obtained: $(RA)_{bulk}$ = 6.8 Ω × cm^2, $R_{surface}$ = 8403 Ω × cm. Figure 5b also shows the temperature dependence of R_bA at reverse biases and the temperature dependence of R_0A according to the empirical model Rule 07.[43] The empirical Rule 07 model was proposed to describe the temperature dependence of the dark current of high-quality MBE HgCdTe photodiodes, in which the dark current is limited by Auger-1 processes. The Rule 07 model is widely used to assess the quality of infrared detectors of various types (including barrier detectors[16]).

It can be seen from Fig. 5b that in a temperature range of 210–300 K, the R_bA values for the fabricated nBn structure excluding surface leakage exceed the values of the similar parameters according to the Rule 07 model. It can be noted that, at reverse biases, the value of the resistance of the barrier layer, determined from measurements of the admittance of MIS devices, in a temperature range of 210 K to 300 K is limited by the diffusion of holes from the absorbing layer, and at lower temperatures, the most probable dominant mechanism is tunneling through traps, and the activation energy in this temperature range is close to 28 meV. It can be noted that Shockley-Read-Hall generation in HgCdTe-based barrier detectors is effectively suppressed since the devices are designed in such a way that depletion regions are located in a wide-gap barrier. Thus, when solving the problem of surface passivation for the barrier layer of $Hg_{0.33}Cd_{0.67}Te$ in nBn structures based on MBE HgCdTe, it is possible to achieve high R_bA values in a temperature range of 210–300 K.

Conclusion

Thus, the electrical properties of mid-wave infrared nBn structures based on HgCdTe MBE with Al_2O_3 passivation were studied, with the composition in the absorbing layer being 0.29 and the composition in the 120 nm thick barrier layer being 0.67. It was shown that the dark current of nBn structures in a wide temperature range is limited by surface leakage. In a wide range of conditions, the admittance of test MIS devices based on nBn structures was studied. An equivalent circuit of an MIS device is proposed, which allows one to describe the experimental frequency dependence of the impedance.

It is shown that the values of the R_bA product found from the frequency dependence of the impedance of MIS devices based on nBn structures are determined by the bulk component of the current, since the influence of the surface leakage current is excluded in such systems. It has been established that the temperature dependence of the dynamic resistance of the barrier in a temperature range of 230–300 K under forward bias is determined by the diffusion of holes from the contact layer, and under reverse bias by the diffusion from the absorbing layer. It is shown that the values of the R_bA product at reverse biases in a temperature range of 210–300 K exceed the values of a similar parameter calculated according to the empirical model Rule 07. Thus, in solving the surface leakage problem for the $Hg_{0.33}Cd_{0.67}Te$ barrier layer with the selected parameters of the multilayer unipolar system, it is possible to create an MWIR detector with high R_bA values over a wide temperature range.

Acknowledgements The work was supported by the Russian Science Foundation (Grant No. 19-12-00135).

Declarations

Conflict of interest The authors declare that they have no conflict of interest.

References

1. M.A. Kinch, *J. Electron. Mater.* **44**, 2969 (2015).
2. D.A. Reago, S.B. Horn, J. Campbell Jr., and R.H. Vollmerhausen, *Proc. SPIE* **3701**, 108 (1999).
3. A. Rogalski, J. Antoszewski, and L. Faraone, *J. Appl. Phys.* **105**, 4 (2009).
4. S. Maimon and G.W. *Appl. Phys. Lett.* **89**, 151109 (2006).

5. A. Rogalski, *Infrared and Terahertz Detectors*, 3rd edn. (CRC Press, Boca Raton, 2019).
6. D.Z. Ting, A. Soibel, A. Khoshakhlagh, S.B. Rafol, S.A. Keo, L. Höglund, A.M. Fisher, E.M. Luong, and S.D. Gunapala, *Appl. Phys. Lett.* **113**, 021101 (2018).
7. M. Delmas, R. Rossignol, J.B. Rodriguez, and P. Christol, *Superlattice Microstruct.* **104**, 402 (2017).
8. A. Evirgen, J. Abautret, J.P. Perez, A. Cordat, A. Nedelcu, and P. Christol, *Electron. Lett.* **50**, 1472 (2014).
9. N.D. Akhavan, G.A. Umana-Membreno, R. Gu, J. Antoszewski, and L. Faraone, *IEEE Trans. Electron Dev.* **65**, 591 (2018).
10. F. Uzgur and S. Kocaman, *Proc. SPIE* **11129**, 1112903 (2019).
11. D. Benyahia, P. Martyniuk, M. Kopytko, J. Antoszewski, W. Gawron, P. Madejczyk, J. Rutkowski, R. Gu, and L. Faraone, *Opt. Quantum Electron.* **48**, 215 (2016).
12. J. He, P. Wang, Q. Li, F. Wang, Y. Gu, C. Shen, L. Chen, P. Martyniuk, A. Rogalski, X. Chen, W. Lu, and W. Hu, *IEEE Trans. Electron Dev.* **67**, 2001 (2020).
13. A.M. Itsuno, J.D. Phillips, and S. Velicu, *Appl. Phys. Lett.* **100**, 161102 (2012).
14. A.M. Itsuno, J.D. Phillips, and S. Velicu, *J. Electron. Mater.* **41**, 2886 (2012).
15. O. Gravrand, F. Boulard, A. Ferron, P. Ballet, and W. Hassis, *J. Electron. Mater.* **44**, 3069 (2015).
16. M. Kopytko and A. Rogalski, *Prog. Quantum Electron.* **47**, 1 (2016).
17. A.V. Voitsekhovskii, S.N. Nesmelov, S.M. Dzyadukh, S.A. Dvoretsky, N.N. Mikhailov, G.Y. Sidorov, and M.V. Yakushev, *Infrared Phys. Technol.* **102**, 103035 (2019).
18. A.V. Voitsekhovskii, S.N. Nesmelov, S.M. Dzyadukh, S.A. Dvoretsky, N.N. Mikhailov, G.Y. Sidorov, and M.V. Yakushev, *J. Phys. D: Appl. Phys.* **53**, 055107 (2019).
19. E. Gomółka, M. Kopytko, O.K. Markowska, K. Michalczewski, L. Kubiszyn, A. Kębłowski, J. Jureńczyk, W. Gawron, P.M. Martyniuk, J.F. Piotrowski, J. Rutkowski, and A. Rogalski, *Opt. Eng.* **57**, 027107 (2018).
20. X. Hao, Y. Zhao, Q. Wu, X. Li, Y. Teng, M. Xiong, Y. Huang, B. Chen, J. Huang, Z. Deng, and H. Yang, *Semicond. Sci. Technol.* **34**, 065013 (2019).
21. X. Du, B.T. Marozas, G.R. Savich, and G.W. Wicks, *J. Appl. Phys.* **123**, 214504 (2018).
22. D.E. Sidor, G.R. Savich, and G.W. Wicks, *J. Electron. Mater.* **45**, 4663 (2016).
23. M. Kopytko, E. Gomółka, K. Michalczewski, P. Martyniuk, J. Rutkowski, and A. Rogalski, *Semicond. Sci. Technol.* **33**, 125010 (2018).
24. C.P. Morath, E.A. Garduno, G.D. Jenkins, E.A. Steenbergen, and V.M. Cowan, *Infrared Phys. Technol.* **97**, 448 (2019).
25. X.M. Shen, ZYu. He, S. Liu, ZYu. Lin, Y.H. Zhang, D.J. Smith, and M.R. McCartney, *Appl. Phys. Lett.* **107**, 122109 (2015).
26. N. Yoon, C.J. Reyner, G. Ariyawansa, J.M. Duran, J.E. Scheihing, J. Mabon, and D. Wasserman, *J. Appl. Phys.* **122**, 074503 (2017).
27. D.R. Rhiger and E.P. Smith, *J. Electron. Mater.* **48**, 6053 (2019).
28. C.Y. Tsai, Y. Zhang, Z. Ju, and Y.H. Zhang, *Appl. Phys. Lett.* **116**, 201108 (2020).
29. J. Kim, H. Yuan, J. Kimchi, J. Lei, E. Rangel, P. Dreiske, and A. Ikhlassi, *Proc. SPIE* **10624**, 1062412 (2018).
30. K. Michalczewski, F. Ivaldi, L. Kubiszyn, D. Benyahia, J. Boguski, A. Kębłowski, P. Martynuk, J. Piotrowski, and A. Rogalski, *Acta Phys. Pol. A* **132**, 325 (2017).
31. X. Li, D. Jiang, Y. Zhang, D. Wang, Q. Yu, T. Liu, H. Ma, and L. Zhao, *J. Phys. D: Appl. Phys.* **49**, 165105 (2016).
32. D.R. Rhiger, E.P. Smith, B.P. Kolasa, J.K. Kim, J.F. Klem, and S.D. Hawkins, *J. Electron. Mater.* **45**, 4646 (2016).
33. A. Glasmann, I. Prigozhin, and E. Bellotti, *IEEE J. Electron Device Soc.* **7**, 534 (2019).
34. A.V. Voitsekhovskii, S.N. Nesmelov, S.M. Dzyadukh, S.A. Dvoretsky, N.N. Mikhailov, G.Y. Sidorov, and M.V. Yakushev, *Mater. Res. Expr.* **6**, 116411 (2019).
35. A.V. Voitsekhovskii, S.N. Nesmelov, S.M. Dzyadukh, S.A. Dvoretsky, N.N. Mikhailov, G.Y. Sidorov, and M.V. Yakushev, *Semicond. Sci. Technol.* **35**, 055026 (2020).
36. R. Rossignol, J.B. Rodriguez, Q. Durlin, H. Aït-Kaci, J.P. Perez, F. Martinez, F. Gonzales Posada, and P. Christol, *Proc. SPIE* **10111**, 101111H (2017).
37. I.I. Izhnin, A.V. Voitsekhovskii, S.N. Nesmelov, S.M. Dzyadukh, S.A. Dvoretsky, N.N. Mikhailov, G.Y. Sidorov, and M.V. Yakushev, *Appl. Nanosci.* (2021). https://doi.org/10.1007/s13204-020-01636-z.
38. Y.G. Sidorov, S.A. Dvoretskii, V.S. Varavin, N.N. Mikhailov, M.V. Yakushev, and I.V. Sabinina, *Semiconductors* **35**, 1045 (2001).
39. R. Fu and J. Pattison, *Opt. Eng.* **51**, 104003 (2012).
40. P. Zhang, Z.H. Ye, C.H. Sun, Y.Y. Chen, T.N. Zhang, X. Chen, C. Lin, R.J. Ding, and L. He, *J. Electron. Mater.* **45**, 4716 (2016).
41. S. Velicu, J. Zhao, M. Morley, A.M. Itsuno, and J.D. Phillips, *Proc. SPIE* **8268**, 82682X (2012).
42. N.D. Akhavan, G. Jolley, G.A. Umana-Membreno, J. Antoszewski, and L. Faraone, *J. Electron. Mater.* **44**, 3044 (2015).
43. W.E. Tennant, D. Lee, M. Zandian, E. Piquette, and M. Carmody, *J. Electron. Mater.* **37**, 1406 (2008).